Minimizing Coherent Thermal Conductance by Controlling the Periodicity of Two-Dimensional Phononic Crystals

Yaolan Tian, Tuomas A. Puurtinen, Zhuoran Geng, and Ilari J. Maasilta*
Nanoscience Center, Department of Physics, University of Jyvaskyla, P.O. Box 35, FIN-40014 Jyvaskyla, Finland

(Received 17 December 2018; revised manuscript received 19 April 2019; published 3 July 2019)

Periodic hole-array phononic crystals (PnCs) can strongly modify phonon dispersion relations and have been shown to influence thermal conductance coherently, especially at low temperatures where bulk scattering is suppressed. One very important parameter influencing this effect is the period of the structure. Here, we measure the subkelvin thermal conductance of nanofabricated PnCs with identical hole-filling factors but three different periodicities, of 4, 8, and 16 μm, using superconducting tunnel-junction thermometry. We find that all the measured samples can suppress thermal conductance by an order of magnitude and have a lower thermal conductance than the previously measured smaller-period 1-μm and 2.4-μm structures. The 8-μm-period PnC gives the lowest thermal conductance of all the above samples and has the lowest specific conductance per unit heater length observed to date in PnCs. In contrast, coherent transport theory predicts that the longest period should have the lowest thermal conductance. Comparison with incoherent simulations suggests that diffusive boundary scattering is likely the mechanism behind the partial breakdown of the coherent theory.

DOI: 10.1103/PhysRevApplied.12.014008

I. INTRODUCTION

The engineering of phonon thermal transport is a topic with a wide current interest, with applications such as improving the heat dissipation out of electronic devices [1], reducing the parasitic phonon thermal-conductance channel in thermoelectric devices [2], using heat in phononic information processing [3], and increasing the sensitivity of low-temperature bolometric detectors [4,5]. Traditionally, the reduction of thermal conductivity is realized by the introduction of disorder, impurities, nanoparticles, rough surfaces, etc. [6], thus increasing the diffusive scattering of thermal phonons. At subkelvin temperatures, for example, simply roughening the surfaces of a thin plate has been predicted to lead to ultralow thermal conductance that is relevant for ultrasensitive radiation-detector applications [4,7] or, at room temperature, thin native oxides at the surface can increase the scattering significantly [8]. On the other hand, an interesting question is whether thermal conductance can also be modified by changes in the dispersion relations or the band structure of phonons [9,10].

One way to achieve a strong modification of phonon dispersion is by artificially introducing periodic modification of the elastic properties of the materials in the length scale corresponding to the phonon-wavelength range of interest [11,12]. These structures are known as phononic crystals (PnCs) [13,14] and, depending on the contrast between elastic parameters and dimensionality, even complete band gaps can form at certain frequency ranges, due to Bragg interference [13,14]. One clear choice for a PnC structure in two dimensions is thus a periodic array of holes, where the simple geometry of a square array of circular holes already creates strong effects [15]. Such geometries have been applied in studies of thermal conductivity mostly at room temperature and somewhat below [16–23] or above [24] and with periodicities in the 10 nm to 1 μm length scale. The full theoretical understanding and interpretation of such experiments is still debated and ongoing, mostly because of the sensitivity to sample details [25], the varying mean free paths of different-wavelength phonons in the broad thermal spectrum [26–29], and the complex interplay between incoherent and coherent scattering [25,30]. It is certainly clear that coherent effects are not guaranteed at high temperatures and at 100 nm $-$ 1 μm length scales, as the wavelengths of dominant phonons at room temperature are typically approximately 10 nm. Recent experiments comparing ordered and disordered hole arrays indeed seem to indicate that coherent effects wash out above 10 K at PnCs of period 100–300 nm [22,23].

To solve some of these complications, we have shown that at subkelvin temperatures, coherent effects can be dominant in hole-array PnCs [9] and that thermal conductance can be reduced by over an order of magnitude with a 2.4-μm-period PnC with a hole-filling factor of 0.7. Further studies with a 4-μm-period structure have shown even stronger reduction [4]. In addition, coherent effects

*maasilta@jyu.fi

have also been predicted to strongly modify subkelvin heat capacity [31]. Coherent effects are possible because, first, bulk phonon scattering is suppressed [32,33] and thermal phonons can travel ballistically for very long distances in thin (1 μm and less) membranes with smooth surfaces, up to distances of approximately $0.1 - 1.0$ mm [34–36]. Second, the dominant thermal wavelengths are increased by three orders of magnitude compared to room temperature and can reach values above 1 μm. Moreover, the high-frequency phonons are completely frozen; for example, 99% of phonons in silicon nitride have frequencies below 20 GHz and such low-frequency phonons have been experimentally shown to retain coherence in hypersonic-acoustic-wave experiments [21] and in Brillouin-scattering measurements for thermally populated phonons [37]. Thus, subkelvin-temperature phonons are ideally suited for coherent modification of thermal conductance and it has already been demonstrated that micron-scale periodic structures can have a strong effect [9].

It has also become clear that a possible phononic band gap is not the main reason for the reduction of thermal conductance in the two-dimensional (2D) hole-array structures but that it is the modifications of the density of states (DOS) and the group velocity that are dominant [9,38] and that the period strongly modifies both [9,38,39]. Specifically, the band structures are modified in such a way that with increasing period, the average group velocity decreases significantly, leading to the counterintuitive effect that the thermal conductance decreases with increasing period (increasing neck size), in contrast to incoherent-boundary-scattering models where the conductance increases with the neck size [40,41]. The coherent theory [38] does not predict a saturation or reversal of this effect up to periods of 8 μm. However, in real samples with nonzero diffusive boundary scattering, an interplay between coherent and incoherent phonon populations could lead to an eventual reversal of the trend. Thus, there should be a practical limit giving the minimum thermal conduction as a function of the periodicity of the PnC.

Here, we measure the subkelvin thermal conductance of 2D square-lattice hole-array phononic crystal structures made from 300-nm-thick silicon nitride membranes, similar to devices in Refs. [4,9] but with much longer periods of 4 μm, 8 μm, and 16 μm, keeping the hole-filling factor constant at 0.7 (Fig. 1). We observe that out of those structures, the 8 μm period has the lowest thermal conductance, showing that the model of fully coherent and ballistic phonon transport starts to break down beyond that periodicity. The numerical modeling performed suggests that diffusive surface scattering at the hole side walls is likely responsible for this breakdown. In addition, we compare two PnC structures with the same 8-μm period but a different heater length and see that a ballistic model for the heat exchange between the heater and the thermometer can explain the observations of how the measured thermal conductance depends on the heater and thermometer geometry.

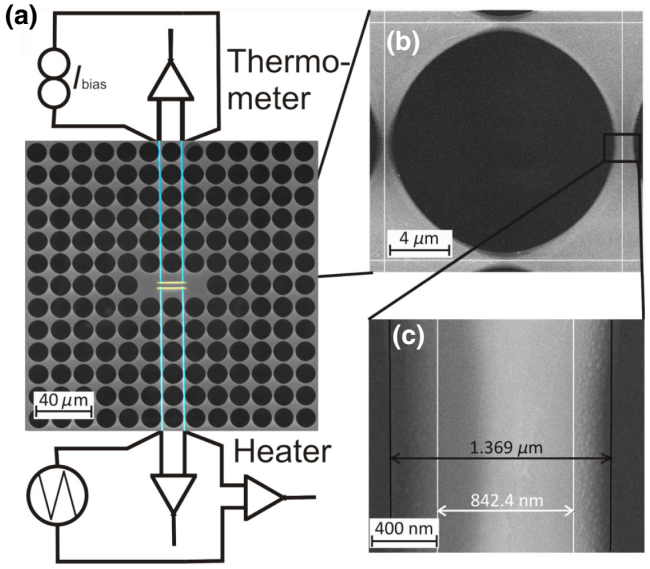

FIG. 1. Scanning electron micrograph (SEM) images of 2D PnC structures with a periodicity of 16 μm. (a) A larger-scale image of the PnC, showing the central region with the heater and thermometer (yellow), with superconducting leads (blue) extending up and down. The measurement setup is also schematically shown. (b) An enlargement of one hole. (c) A enlargement of a neck region between two holes. The dimensions show the width of the top (white) and bottom (black) neck regions. Their difference indicates sloping side walls, with roughness on them being visible.

II. THEORETICAL MODELING

Before we show the experimental results, we discuss the theoretical modeling. The band structures of 4-μm-, 8-μm-, and 16-μm-period hole-array 2D phononic crystals, corresponding to the experiment, are calculated by solving the three-dimensional (3D) elasticity equations for an isotropic material [42] with SiN parameters (Young's modulus $E = 250$ GPa, Poisson ratio $\nu_p = 0.23$, and density $\rho = 3100$ kg/m^3) using the finite-element method (FEM). Periodic Bloch-wave boundary conditions are used with 2D wave vectors $\mathbf{k}$ in the x-y plane, typically with approximately $500 - 1000$ k points in the irreducible octant of the first Brillouin zone (BZ). Depending on the value of the PnC period, approximately $16\,000 - 87\,000$ eigenvalues are computed, extending the frequency range to at least 40 GHz for all periodicities. Unperforated membrane results are also calculated, with the help of the Rayleigh-Lamb theory [42,43].

In Fig. 2, we compare the dispersion relations of the three PnC structures, shown in the symmetry directions Γ-X-M-Γ only up to a frequency $\nu = 2$ GHz for clarity.

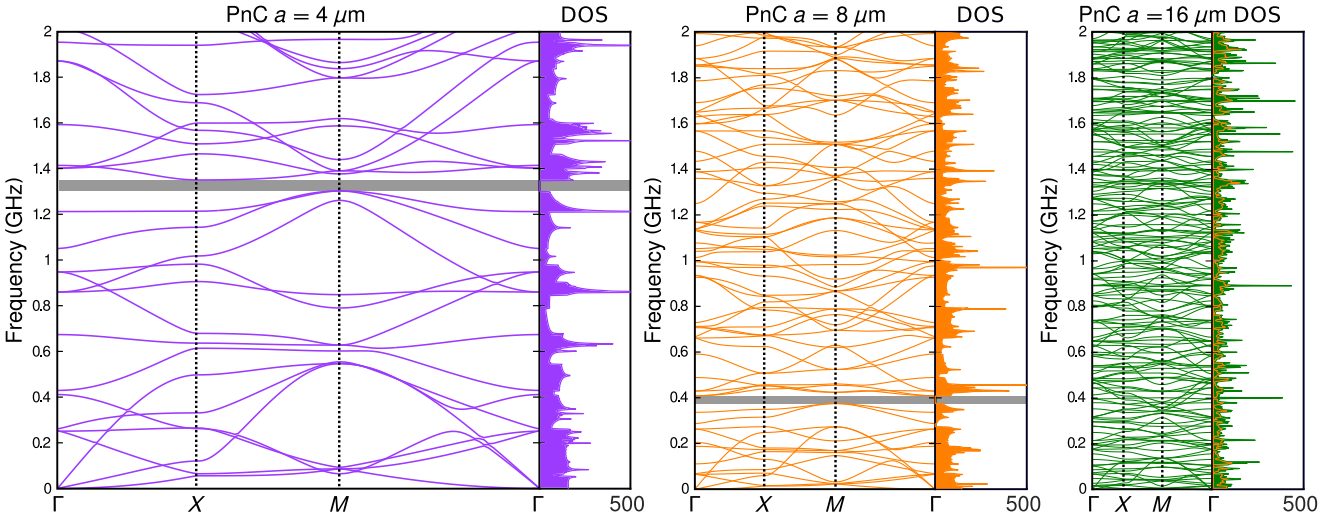

FIG. 2. The densities of states and dispersion relations (band structure) in the main symmetry directions of the Brillouin zone (BZ) for the SiN square-lattice hole-array PnC of thickness 300 nm and hole-filling factor 0.7, with periodicity (left) $a = 4$ μm, (middle) $a = 8$ μm, and (right) $a = 16$ μm. A complete band gap is observable at $\nu = 1.3$ GHz for the PnC with $a = 4$ μm and at $\nu = 0.4$ GHz for the PnC with $a = 8$ μm.

Full 2D band structures are computed for thermal conductance calculations. It is evident that there are great differences between the band structures: the number of bands increases with the periodicity but the bands become also much flatter. The 4-μm-(8-μm-)period PnC has a complete band gap at 1.3 GHz (0.4 GHz) but its effect is expected to be minor as it only occupies a small frequency region compared to the full thermal bandwidth, which is around 20 GHz even at 0.1 K. The flatness of the bands will affect both the group velocities $\partial\omega/\partial k$ and the DOS (shown in Fig. 2) but at this scale of periodicity, the main effect on coherent thermal conduction comes from the reduction of the average group velocity [38].

To calculate the phonon emission from the heater, we take the outward-propagating phonon modes (mode index j and wave vector $\mathbf{k}$) with energies $\hbar\omega_j(\mathbf{k})$, and derive [9,38] the following relation for the radiated power for both PnCs and uncut membranes:

$$P(T) = \frac{1}{(2\pi)^2}\sum_j \oint_\gamma d\gamma \times \int_K d\mathbf{k}\hbar\omega_j(\mathbf{k}) n \frac{\partial\omega_j}{\partial\mathbf{k}}\cdot\hat{n}_\gamma \Theta\left(\frac{\partial\omega_j}{\partial\mathbf{k}}\cdot\hat{n}_\gamma\right), \quad (1)$$

where γ is the heater-element boundary, $\hat{n}_\gamma$ is an outer unit normal of that boundary (in the membrane plane), and Θ is the Heaviside step function. Here, $n = n(\omega, T)$ is the Bose-Einstein distribution describing the (assumed) phonon thermal occupation of the emitted phonons and $\partial\omega_j/\partial\mathbf{k}$ the group velocity of each mode. The only unknown is thus the set of dispersion relations $\omega_j := \omega_j(\mathbf{k})$ for the permitted phonon modes j in the membrane. The 2D K-space integration extends over all K space for uncut membranes but is replaced by integration over the first Brillouin zone for the PnCs. Equation (1) also assumes that the membrane is infinite, so that there is no backscattering from the membrane-bulk interface, and that the bath is at $T_{\text{bath}} = 0$ K, so that there is no direct backflow term. The backflow from the bath is taken into account in calculations when comparing with the experiments, by writing $P_{\text{net}} = P(T) - P(T_{\text{bath}})$, where $P(T_{\text{bath}})$ is the calculated power at T_{bath}.

Note that due to the group-velocity term, it is *not* possible in general to simplify the above equation to be just an integral over energies weighed by the DOS. This is because the PnC structures are not isotropic, so that the group velocity is not a constant on a constant-energy surface.

III. EXPERIMENTAL RESULTS AND DISCUSSION

The measurement is performed with a heater and a thermometer pair at the center of the PnC structure (Fig. 1), by measuring how the temperature of the thermometer rises with the dissipated power at the heater (the emitted phonon power). This is achieved by using two normal metal-insulator-superconductor (NIS) tunnel-junction pairs in series (SINIS junctions), both as a thermometer [44,45] and as a heater [46,47]. In contrast to our earlier measurements [4,9], where Cu was used as the normal metal, here we use Au-Ti bilayers as the normal metal. This is because Au-Ti has been found to be a more robust material; in particular, it survives the contact with polymer resists and solvents in the following lithography steps much better than Cu, increasing the fabrication yield. More

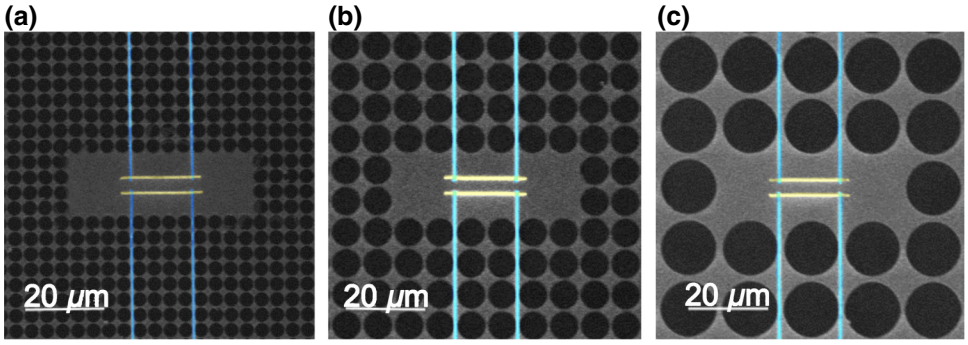

FIG. 3. SEM images of the three different-period SiN PnC structures measured, all with a membrane thickness of 300 nm and a hole-filling factor of 0.7: (a) $a = 4$ μm; (b) $a = 8$ μm; (c) $a = 16$ μm. The yellow shows the normal-metal regions and the blue the superconducting leads.

details on the fabrication and the measurement setup are given in Appendix A.

The power vs temperature curves are measured for the three different PnC structures with 4 μm, 8 μm, and 16 μm periods, shown in Fig. 3. As can be seen, the heater and thermometer geometry is identical in all samples and the platform area without the holes about the same. We thus minimize the influence of other factors except for the periodicity of the PnC.

For the three different-period PnC structures, the measured power vs phonon temperature data are shown in Fig. 4(a). The membrane thickness (300 nm) and the hole-filling factor (0.7) are kept constant. In addition, a measurement of an uncut membrane of the same thickness and with the same heater and thermometer geometry is shown. The bath temperature is stable in each measurement but varies between measurements in the range 55–78 mK for the PnC data, and is 95 mK in the case of the membrane.

Clearly, the emitted phonon power in all the PnC samples is about an order of magnitude below the uncut membrane; in other words, the thermal conductance is strongly reduced in the PnC structure. Interestingly, the 8-μm PnC has the lowest thermal conductance of all the measured samples, showing that there is a limit for how much it can be reduced simply by increasing the period with coherent band-structure modification. For these types of devices, the optimum period for minimizing G therefore lies between 4 μm and 16 μm. This ordering is in stark contrast with the calculations based on Eq. (1), also shown in Fig. 4, which predict that G should continue to decrease with an increasing period. Classically [48], if the medium is diffusive, all the PnC structures would have the same thermal conductance, as it would then only depend on the hole-filling factor. On the other hand, in the boundary-scattering-limited models, an increase of G with the period is to be expected, as the neck size is increasing [40,41]. Nonmonotonous behavior is thus an indication of

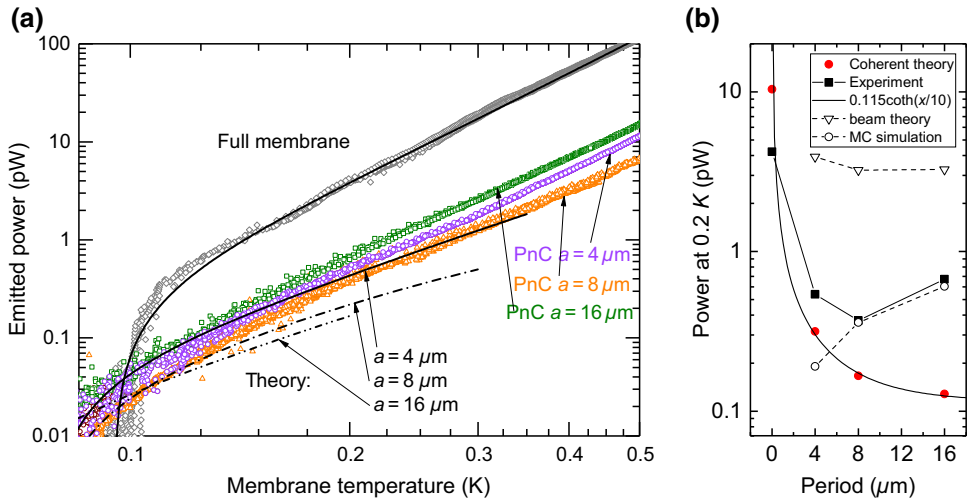

FIG. 4. (a) Measured power vs temperature for the 4-μm- (purple circles), 8-μm- (orange triangles), and 16-μm- (green squares) period PnCs and for an uncut membrane with the same heater geometry (gray diamonds). The lines (solid, full membrane and 4 μm; dot-dash, 8 μm; dot-dot-dash, 16 μm) are theoretical curves calculated for each structure based on the ballistic model given in Eq. (1). (b) The observed power (black squares), the expected theoretical coherent power (red circles), the theoretical ballistic beam power (triangles), and the Monte Carlo (MC) simulation with partially diffusive scattering (open circles) at a constant temperature of 0.2 K as a function of the PnC period. Zero period corresponds to a full membrane. The line is a guide to the eye.

TABLE I. The parameters of all square-lattice PnCs measured to date. All samples have a hole-filling factor of 0.7. Here, "Material" refers to the heater and thermometer normal-metal material, a is the PnC period, t is the membrane thickness, L is the heater and thermometer normal-metal length, and G is the measured thermal conductance.

Material	a (μm)	t (nm)	L (μm)	G(0.2 K) (pW/K)	G(0.2 K)/L [pW/(K μm)]	Ref.
Cu	0.97	485	10	31.4	3.1	[9]
Cu	2.4	485	10	11.6	1.2	[9]
Cu	4	300	8	4.0	0.5	[4]
AuTi	4	300	8	2.8	0.35	
AuTi	4	300	16	4.5	0.28	
AuTi	8	300	16	3.2	0.20	
AuTi	16	300	16	4.6	0.28	

the breakdown of coherence and the increased importance of boundary scattering.

For quantitative results, we define the thermal conductance as $G = P/(T - T_{\text{bath}})$ and obtain experimental values of 4.5, 3.2, and 4.6 pW/K for the 4-, 8-, and 16-μm-PnC structures at $T = 0.2$ K. The PnC values are very low (comparable to a four-beam quantized thermal conductance [49] of 3 pW/K at 0.2 K), with the 8 μm result being the lowest observed specific conductance (independent of heater length) $G/L = 0.2$ pW/(Kμm) for any PnC so far (Table I). The values are also quite close to what has been measured before [4] for a 4-μm structure with a different heater and thermometer length and material. However, the membrane result is about an order of magnitude below what was observed in Refs. [4,9], so that the apparent reduction of G now looks smaller. This observation is not fully understood but clearly results from the variations of the measurements in uncut membranes and not those of the PnCs. It is possible that G in the membranes is much more prone to nonidealities, roughness variations, surface oxides, resist residues, etc. and that the heater and thermometer geometry and material choice have a stronger effect in the uncut membranes. More work on this issue is clearly desirable.

In light of this, we plot the theoretical curves for the PnC structures [based on the FEM-calculated band structures and ballistic power; Eq. (1)] in Fig. 4(a) in such a way that the 4-μm data are fitted and the 8- and 16–μm curves use the same absolute scaling factor. In this way, we can see that below 0.15 K, the 8-μm structure initially follows the thermal-conductance reduction predicted by the theory but later starts to deviate upward, as do the 4-μm data at a slightly higher temperature around 0.2 K. On the other hand, the 16-μm structure does not follow the predicted reduction at all and has about five times higher conductance around 0.2 K than the theory predicts.

If we study Fig. 4(a) in more detail, we see that the temperature dependence of the emitted power is quite different between the uncut membrane and all the PnC samples, as has been observed before [4,9]. For the membrane, we have $P \sim T^{3.8}$ at the higher T range, which is fully consistent with the ballistic Rayleigh-Lamb theory, as can be seen by the nearly perfect fit of the theoretical curve. This is expected, as the crossover from Rayleigh-Lamb modes to 3D bulk modes is estimated to take place at a membrane thickness of approximately 1 μm for SiN [50]. In contrast, the temperature exponents are lower for the PnC structures, at around 3.0–3.4. Comparing with the theory, we see that the temperature dependencies agree with the theory at the low-temperature end but start to deviate at higher temperatures. Both the deviations of the magnitude and the temperature dependence thus lead to the conclusion that coherence can be destroyed by increasing the period beyond approximately 8 μm or by increasing the temperature.

To make the deviations from the fully coherent theory more clear, we also plot the observed power and expected theoretical power at a constant temperature in Fig. 4(b), as a function of the PnC period. The theoretical points are now presented without any fitting procedure and take into account a geometrical correction due to the heater and thermometer dimensions (see the Supplemental Material [51]). We observe that for all the PnC devices, the experimental power is higher than is predicted by the coherent theory, which cannot be explained by adding a finite emissivity factor to Eq. (1), as it could only reduce the amount of phonon emission from the heater. The experimental reduction between the 4- and 8-μm PnCs follows the coherent-theory trend but the 16-μm data show an increase rather than a decrease, which is again a strong indication of at least a partial breakdown of the coherent picture.

It is also possible to consider models where the coherence has been destroyed fully or partially. In the first model (see the Supplemental Material [51]), we consider the case in which the coherence length is longer than the cross-section neck dimensions but shorter than the periodicity. In such a case, the phonon modes carrying heat are defined by the set of quasi-one-dimensional (1D) beams leading out of the heated platform. Figure 4(b) also shows the expected power in that case, assuming no backscattering.

We observe that the expected power level in such a model is an order of magnitude higher than the experimental observations, and thus describes the experimental data poorly.

Another model considers the full destruction of coherence, in which case phonons behave as particles, without the formation of new modes due to wave interference. Such a situation can be simulated with well-known Monte Carlo (MC) techniques [52,53]. We perform such simulations (detailed in Appendix B) using a code developed in Ref. [22]. As an example, theoretical points based on a MC simulation with a specular scattering probability $p = 0.95$ from the hole side walls are also shown in Fig. 4(b). We observe that, indeed, such a model predicts the increasing trend seen for the longer-period structures, in contrast to the prediction of the fully coherent theory. Although our model is crude and contains several unknown parameters, it lends support to the idea that the total conductance is a sum of a coherent and an incoherent contribution. As the coherent contribution gets smaller with the periodicity and the incoherent one behaves in the opposite manner, nonmonotonous behavior can result, where at smaller periods the coherent theory dominates but at the larger periods the incoherent theory is the more dominant contribution.

The evidence for partially diffusive boundary scattering can also be strengthened by pointing out that the observed side-wall roughness scale [approximately 7 nm from SEM images such as Fig. 1(c)] indeed gives a finite diffusive scattering probability [54–56] for the dominant thermal Lamb-wave modes in the temperature range of the experiment (see the Supplemental Material [51]). Note that the observed rms side-wall roughness stays constant between the different samples, as the fabrication recipe stays the same. Thus, the observed effects are interpreted to arise from the direct effect of the geometry (the neck size).

Finally, as the coherent theory is formulated in the ballistic regime, we can also build simple models (see the Supplemental Material [51]) of how the heater and thermometer geometry influences the measurement, in analogy with radiative photonic heat-transfer problems [57]. By modeling the heater and thermometer geometry with two parallel wires, it is possible to derive analytical expressions for the view factors, set the power-balance equations, and solve numerically for both the temperature of the heater and the thermometer as a function of the dissipated power in the heater. This means that Eq. (1), where only the heater temperature appears, can be extended to situations in which the heater and thermometer temperatures are not equal, with both the heater and the thermometer explicitly taken into account in the effective phonon emission into the PnC. For our geometry, the result is a correction term of magnitude approximately 20%, as discussed in the Supplemental Material [51].

To test such modeling further, in Fig. 5, we compare two measurements, both on a 4-μm-period PnC but with different lengths of the AuTi heater and thermometer structures, one of 8 μm and the other of 16 μm. In the diffusive limit, the heater and thermometer temperature should scale with P/L, the power per unit length of the heater, predicting a constant-scale-factor difference of 2 between the two measurements. Looking at the data, no such simple factor is observed, in contrast, the two measurements give quite similar results at low temperatures of $T < 0.2$ K but deviate more strongly at higher temperatures. In contrast, the ballistic two-wire model explains the power reduction in the shorter heater and thermometer structure very well, as shown by Fig. 5. The partially incoherent ballistic 1D beam theory, on the other hand, predicts no dependence on the heater length at all, which does not agree with the experiment.

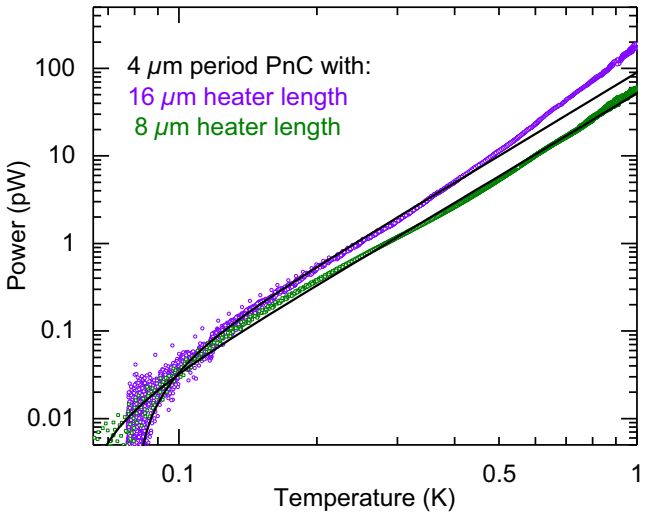

FIG. 5. The measured power vs the temperature for two 4-μm-period PnCs, one with a AuTi heater and thermometer length of 8 μm (green squares) and the other of 16 μm (purple circles). The theoretical line for the longer 16-μm heater structure is calculated by the parallel wire model and used to determine the parameters (fit), whereas the line describing the 8-μm structure is calculated without fitting, by keeping all other parameters fixed and by just changing the wire length.

IV. CONCLUSIONS

In conclusion, we measure the thermal conductance of three 2D square-lattice hole-array phononic crystal structures in the subkelvin temperature range, between the periodicities 4 and 16 μm, which are much larger than in previous work [4,9]. The thermal conductance is still strongly reduced by the PnC structures, similar to Refs. [4,9], and we demonstrate a record low specific conductance of 0.2 pW/(Kμm) for 2D phononic crystals. However, the largest period no longer gives the lowest thermal conductance, as predicted by the fully coherent theory. The observed nonmonotonous behavior as a function of

the period can be explained by the interplay of coherent and incoherent phonon populations, with the incoherent component becoming more dominant as the period grows. A practical limit thus seems to exist on the periodicity scale that the coherent conductance dominates, depending on the details of the samples (such as surface roughness). In our structures, this limit is roughly at the 10 μm scale.

In addition, a temperature increase seems to start to destroy coherence as well. This is to be expected, since higher temperatures excite higher-frequency phonons, which have stronger diffusive scattering probabilities than lower-frequency phonons. In the future, if the 2D specific thermal conductance G/L needs to be reduced below 0.2 pW/(Kμm) levels at 0.2 K, different geometries and strategies need to be employed, and the transition to the incoherent regime could be addressed further by studying the effect of the hole-edge roughness and hole-position disorder. The interpretation outlined in this work suggests that by reducing the roughness, the range of validity of the coherent theory could be extended to larger periodicities and thus to smaller conductances.

Our findings for the level of control and low values of thermal conductance are promising for applications in low-temperature ultrasensitive bolometric radiation detectors [58], where coherent thermal control has the benefit of achieving the required low thermal conductance values with simple, compact, and robust designs. This is in contrast to more traditional methods relying on diffusive surface scattering, where very long and fragile devices have to be used to obtain ultralow conductance values, making parameter control hard and high packing density a challenge.

ACKNOWLEDGMENTS

This study was supported by the Academy of Finland Project Number 298667 and the China Scholarship Council. We thank C. Dames and G. Wehmeyer for sharing the Monte Carlo code. The computational facilities provided by the CSC-IT Center for Science Ltd. are acknowledged.

APPENDIX A: MATERIALS AND METHODS

1. Sample fabrication

All SINIS junctions are deposited on 300-μm-thick single-crystal (100) silicon wafers, coated on both sides with 300-nm-thick low-stress silicon nitride films (Berkeley Nanofab). Silicon nitride membranes of area about 300 μm by 300 μm are fabricated by the standard KOH etching process, in the same way as in Ref. [9] but excluding any tuning of the membrane thickness, i.e., the SiN membrane surfaces are kept in their native state. The heater and the thermometer SINIS junction pairs are then fabricated at the center of the SiN membrane [Fig. 1(a)]. The distance between the heater and the thermometer is set to 4 μm for all samples, shorter than in Ref. [9] but the same as in Ref. [4]. The distance between the two superconducting leads of each SINIS pair is set to 16 μm, i.e., the heater length is about 16 μm, while it is half the length, 8 μm, in Ref. [4]. This heater length is adjusted to fit all the periods chosen, so that we can make a perfect PnC structure, avoiding any "phononic waveguide" features around the superconducting leads present in the older sample designs [9]. We do not have any indications that the possible waveguiding had any major impact in the older experiments but when lower levels of thermal conduction are desired, it could start to influence the measurements.

The fabrication of the SINIS junctions is similar to the process in Ref. [4], using electron-beam lithography. Al is used as the superconductor and is deposited by a two-sided angle-evaporation technique from a set of angles of 70, 65, and 60 degrees for each side. This decreasing set of deposition angles is chosen to make sure that each layer is wholly deposited on top of the previous layer. The total Al thickness is 26.5 nm. Then, an *in situ* AlO_x tunnel barrier is formed by thermal oxidation at 200 mbar of oxygen for 5 min.

After a rotation of 90 degrees, a thin Ti adhesion layer is deposited from an angle of 70 degrees on both sides, with a total thickness of 10 nm. Without breaking the vacuum, an Au layer of total thickness 37.3 nm is deposited in the same way as the Al. The purpose of this fairly complex high-angle deposition is to avoid the deposition of any normal-metal layers on top of the superconducting leads, as they can influence phonon scattering. Finally after liftoff, two $Al/AlO_x/Ti$-Au-$Ti/AlO_x/Al$ SINIS tunnel-junction pairs with a junction area of approximately 370×500 nm^2 and a typical total tunneling resistance of approximately 10 kΩ are obtained. Note that the tunneling resistances are typically lower than if Cu is used, even with similar oxidation parameters [59].

The PnC structures are fabricated after the SINIS junctions, using electron-beam lithography and reactive ion etching [9]. A square lattice of circular holes is patterned on poly(methyl methacrylate) (PMMA) with a thin 7-nm layer of Al on top to prevent charging. After the removal of Al in NaOH and the development of the resist, it is used as an etch mask for reactive ion etching of the SiN_x membrane, using a mixture of O_2 and CHF_3 in the plasma (ratio 10:1) at a power of 100 W and a pressure of 55 mTorr. The total etching time is divided into four steps (6 min + 6 min + 6 min + 3 min 20 s), so that there is a cooling time between each step. The SINIS junctions are located fully on the central uncut membrane island [Fig. 1(a)] and are therefore protected by PMMA during the plasma etching. From Figs. 1(b) and 1(c), it is clear that some nonidealities in the etching still remain. In particular, the side walls are not straight but sloped and in the sample of Fig. 1, the neck

dimension at the upper surface is approximately 840 nm, but at the bottom it is approximately 1370 nm. In this case, the design value for the hole-filling factor of 0.7 is 900 nm. Sloped side walls with similar roughness are also observed in the 8-μm- and 4-μm-period PnCs.

2. Thermal-conductance measurement

The measurement circuit is also shown in Fig. 1(a). The heater is biased with a battery-powered dc voltage source, which can be swept slowly. Both the heater voltage and current are recorded simultaneously during the bias sweep in a four-probe configuration, using Ithaco 1201 and 1211 preamplifiers, respectively. Thus, the emitted phonon power can be calculated as $P = IV$. Meanwhile, the thermometer SINIS pair is biased by a battery-powered constant-current source and its voltage is measured using another Ithaco 1201 preamplifier as the dissipated power is swept. This voltage is proportional to the phonon temperature T_p and a calibration between voltage and temperature is performed by slowly sweeping the cryostat temperature without any heating power in the heater [9,45].

All measurements are performed in a ^{3}He-^{4}He dilution refrigerator with a base temperature of approximately 50 mK, with several stages of filtering in the wires, because of the extreme sensitivity of the tunnel-junction devices to unwanted spurious power loads. The setup used has pi filters at the 4 K flange and a copper-shielded Eccosorb filter box at the 1 K flange. From 1 K to 50 mK, a set of shielded superconducting wires are used. In addition, 12 stand-alone copper-shielded integrated Eccosorb + LC pi filters with a measured $>$ 80 dB attenuation at 40 MHz-10 GHz are used for each measurement line at the 50 mK sample stage thermalized to T_{bath}.

APPENDIX B: MONTE CARLO SIMULATION OF THE INCOHERENT BOUNDARY-SCATTERING-LIMITED CONDUCTANCE

If coherence is fully destroyed, a model calculation for the thermal conductance through a phononic crystal structure can be performed based on the particle picture of phonons, using the Monte Carlo technique and the Landauer-Büttiker formalism [52,53]. We apply the code developed in Ref. [22] (where full details of the computational implementation can be found) to calculate the average phonon-transmission probabilities $\langle\tau\rangle$ through square-lattice circular-hole phononic crystals with varying periods $2-16$ μm, corresponding to the experiment in the main text (membrane thickness 300 nm, hole-filling factor 0.7) (see Fig. 6). The length of the simulated structure is kept constant at 64 μm. No bulk scattering is included and the top and bottom surfaces are assumed to be fully specular ($S = 1$), whereas for the side walls, the specular scattering probabilities are varied between the fully diffusive ($S = 0$) and the fully specular ($S = 1$) limits.

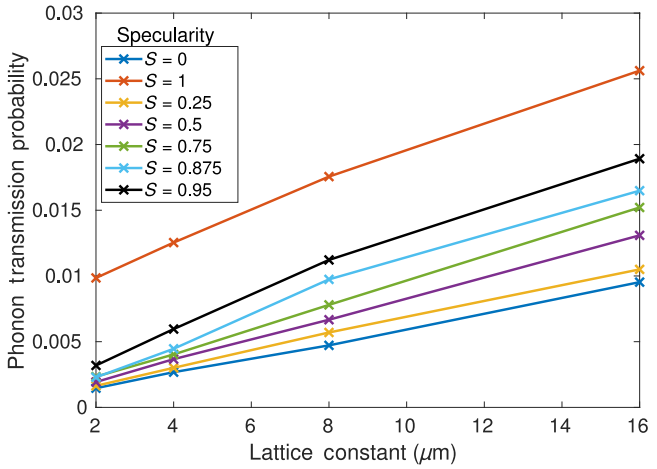

FIG. 6. The calculated average transmission probability of incoherent phonons through square-lattice circular-hole PnCs of varying period and the probability of specular scattering S from the hole side walls. Hole filling factor 0.7, membrane thickness 300 nm, width of the PnC 64 μm.

The transmitted phonon power per unit cross-section area, P/A, is linearly proportional to the average transmission probability $\langle\tau\rangle$ and can be calculated as follows [22,52,53]:

$$P/A = \frac{f}{4}\langle\tau\rangle\sum_i \int d\omega c_i g_i(\omega)\hbar\omega(n_1 - n_2), \qquad \text{(B1)}$$

where f is an unknown fraction of incoherent phonons, the sum runs over the two transverse and one longitudinal bulk-phonon modes with speed of sound c_i, $g_i(\omega)$ is the DOS for mode i, and $n_{1,2}$ are the Bose-Einstein distributions at the two reservoir temperatures in question.

As we see in Fig. 6, for all values of the specularity parameter, the transmission increases with the period, leading to an increase of the thermal conductance, as the power (or conductance) is directly proportional to $\langle\tau\rangle$ [see Eq. B1)]. This can be understood in terms of the geometrical argument of the increasing neck size. Unfortunately, S cannot be estimated from the experiment due to the unknown value of f.

We note that the code used assumes unidirectional heat flow and is therefore an approximation to the full geometry of our experiment, where heat spreads out two-dimensionally into the 2D PnC structure. However, as we are not interested in the exact numbers in the context of this paper but only want to discuss the trend, the simpler simulation is adequate.

[1] S. Volz, J. Ordonez-Miranda, A. Shchepetov, M. Prunnila, J. Ahopelto, T. Pezeril, G. Vaudel, V. Gusev, P. Ruello,

E. M. Weig *et al.*, Nanophononics: State of the art and perspectives, Eur. Phys. J. B **89**, 15 (2016).
[2] A. J. Minnich, M. S. Dresselhaus, Z. F. Ren, and G. Chen, Bulk nanostructured thermoelectric materials: Current research and future prospects, Energy Environ. Sci. **2**, 466 (2009).
[3] N. Li, J. Ren, L. Wang, P. Hänggi, and B. Li, Phononics: Manipulating heat flow with electronic analogs and beyond, Rev. Mod. Phys. **84**, 1045 (2012).
[4] I. J. Maasilta, T. A. Puurtinen, Y. Tian, and Z. Geng, Phononic thermal conduction engineering for bolometers: From phononic crystals to radial Casimir limit, J. Low Temp. Phys. **184**, 211 (2016).
[5] K. Rostem, D. T. Chuss, F. A. Colazo, E. J. Crowe, K. L. Denis, N. P. Lourie, S. H. Moseley, T. R. Stevenson, and E. J. Wollack, Precision control of thermal transport in cryogenic single-crystal silicon devices, J. Appl. Phys. **115**, 124508 (2014).
[6] David G. Cahill, Paul V. Braun, Gang Chen, David R. Clarke, Shanhui Fan, Kenneth E. Goodson, Pawel Keblinski, William P. King, Gerald D. Mahan, Arun Majumdar, Humphrey J. Maris, Simon R. Phillpot, Eric Pop, and Li Shi, Nanoscale thermal transport. II. 2003–2012, Appl. Phys. Rev. **1**, 011305 (2014).
[7] T. A. Puurtinen and I. J. Maasilta, Radial phononic thermal conductance in thin membranes in the Casimir limit: Design guidelines for devices, AIP Adv. **4**, 124503 (2014).
[8] Sanghamitra Neogi, J. Sebastian Reparaz, Luiz Felipe C. Pereira, Bartlomiej Graczykowski, Markus R. Wagner, Marianna Sledzinska, Andrey Shchepetov, Mika Prunnila, Jouni Ahopelto, Clivia M. Sotomayor-Torres, and Davide Donadio, Tuning thermal transport in ultrathin silicon membranes by surface nanoscale engineering, ACS Nano **9**, 3820 (2015).
[9] N. Zen, T. A. Puurtinen, T. J. Isotalo, S. Chaudhuri, and I. J. Maasilta, Engineering thermal conductance using a two-dimensional phononic crystal, Nat. Commun. **5**, 3435 (2014).
[10] M. Maldovan, Phonon wave interference and thermal bandgap materials, Nat. Mater. **14**, 667 (2015).
[11] M. Sigalas and E. N. Economou, Band structure of elastic waves in two dimensional systems, Solid State Commun. **86**, 141 (1993).
[12] M. S. Kushwala, P. Halevi, L. Dobrzynski, and B. Djafar-Rouhani, Acoustic Band Structure of Periodic Elastic Composites, Phys. Rev. Lett. **71**, 2022 (1993).
[13] *Phononic Crystals, Fundamentals and Applications*, edited by A. Khelif and A. Adibi (Springer, Berlin, 2016).
[14] *Acoustic Metamaterials and Phononic Crystals*, edited by P. A.Deymier (Springer, Berlin, 2013).
[15] Y. Pennec, J. O. Vasseur, B. Djafari-Rouhani, L. Dobrzynski, and P. Deymier, Two-dimensional phononic crystals: Examples and applications, Surf. Sci. Rep. **65**, 229 (2010).
[16] J. Tang, H.-T. Wang, D. H. Lee, M. Fardy, Z. Huo, T. P. Russell, and P. Yang, Holey silicon as an efficient thermoelectric material, Nano Lett. **10**, 4279 (2010).
[17] J.-K. Yu, S. Mitrovic, D. Tham, J. Varghese, and J. R. Heath, Reduction of thermal conductivity in phononic nanomesh structures, Nat. Nanotech. **5**, 718 (2010).
[18] P. E. Hopkins, C. M. Reinke, M. F. Su, R. H. Olsson III, E. A. Shaner, Z. C. Leseman, J. R. Serrano, L. M. Phinney, and I. El-Kady, Reduction in the thermal conductivity of single crystalline silicon by phononic crystal patterning, Nano Lett. **11**, 107 (2011).
[19] S. Alaie, D. F. Goettler, M. Su, Z. C. Leseman, C. M. Reinke, and I. El-Kady, Thermal transport in phononic crystals and the observation of coherent phonon scattering at room temperature, Nat. Commun. **6**, 7228 (2015).
[20] Roman Anufriev, Jeremie Maire, and Masahiro Nomura, Reduction of thermal conductivity by surface scattering of phonons in periodic silicon nanostructures, Phys. Rev. B **93**, 045411 (2016).
[21] Markus R. Wagner, Bartlomiej Graczykowski, Juan Sebastian Reparaz, Alexandros El Sachat, Marianna Sledzinska, Francesc Alzina, and Clivia M. Sotomayor Torres, 2D phononic crystals: Disorder matters, Nano Lett. **16**, 5661 (2016).
[22] J. Lee, W. Lee, G. Wehmeyer, S. Dhuey, D. L. Olynick, S. Cabrini, C. Dames, J. J. Urban, and P. Yang, Investigation of phonon coherence and backscattering using silicon nanomeshes, Nat. Commun. **8**, 14054 (2017).
[23] Jeremie Maire, Roman Anufriev, Ryoto Yanagisawa, Aymeric Ramiere, Sebastian Volz, and Masahiro Nomura, Heat conduction tuning by wave nature of phonons, Sci. Adv. **3**, e1700027 (2017).
[24] B. Graczykowski, A. El Sachat, J. S. Reparaz, M. Sledzinska, M. R. Wagner, E. Chavez-Angel, Y. Wu, S. Volz, Y. Wu, F. Alzina, and C. M. Sotomayor Torres, Thermal conductivity and air-mediated losses in periodic porous silicon membranes at high temperatures, Nat. Commun. **8**, 415 (2017).
[25] Navaneetha K. Ravichandran and Austin J. Minnich, Coherent and incoherent thermal transport in nanomeshes, Phys. Rev. B **89**, 205432 (2014).
[26] A. J. Minnich, J. A. Johnson, A. J. Schmidt, K. Esfarjani, M. S. Dresselhaus, K. A. Nelson, and G. Chen, Thermal Conductivity Spectroscopy Technique to Measure Phonon Mean Free Paths, Phys. Rev. Lett. **107**, 095901 (2011).
[27] Jeremy A. Johnson, Jeffrey K. Eliason, Austin J. Minnich, Timothy Kehoe, Clivia M. Sotomayor Torres, Gang Chen, and Keith A. Nelson, Direct Measurement of Room-Temperature Nondiffusive Thermal Transport over Micron Distances in a Silicon Membrane, Phys. Rev. Lett. **110**, 025901 (2013).
[28] K. T. Regner, D. P. Sellan, Z. Su, C. H. Amon, A. J. H. McGaughey, and J. A. Malen, Broadband phonon mean free path contributions to thermal conductivity measured using frequency domain thermoreflectance, Nat. Commun. **4**, 1640 (2013).
[29] Rubina Sultan, A. D. Avery, J. M. Underwood, S. J. Mason, D. Bassett, and B. L. Zink, Heat transport by long mean free path vibrations in amorphous silicon nitride near room temperature, Phys. Rev. B **87**, 214305 (2013).
[30] Ankit Jain, Ying-Ju Yu, and Alan J. H. McGaughey, Phonon transport in periodic silicon nanoporous films with feature sizes greater than 100 nm, Phys. Rev. B **87**, 195301 (2013).
[31] T. A. Puurtinen and I. J. Maasilta, Low temperature heat capacity of phononic crystal membranes, AIP Adv. **6**, 121902 (2016).

[32] J. P. Wolfe, *Imaging Phonons* (Cambridge University Press, Cambridge, 1998).
[33] T. Klitsner, J. E. VanCleve, H. E. Fischer, and R. O. Pohl, Phonon radiative heat transfer and surface scattering, Phys. Rev. B **38**, 7576 (1988).
[34] W. Holmes, J. M. Gildemeister, and P. L. Richards, Measurements of thermal transport in low stress silicon nitride films, Appl. Phys. Lett. **72**, 2250 (1998).
[35] H. F. C. Hoevers, M. L. Ridder, A. Germeau, M. P. Bruijn, P. A. J. de Korte, and R. J. Wiegerink, Radiative ballistic phonon transport in silicon-nitride membranes at low temperatures, Appl. Phys. Lett. **86**, 251903 (2005).
[36] J. T. Karvonen, T. Kühn, and I. J. Maasilta, Temperature profile for ballistic and diffusive phonon transport in a suspended membrane with a radially symmetric heat source, Chin. J. Phys. **47**, 435 (2011).
[37] B. Graczykowski, M. Sledzinska, F. Alzina, J. Gomis-Bresco, J. S. Reparaz, M. R. Wagner, and C. M. Sotomayor Torres, Phonon dispersion in hypersonic two-dimensional phononic crystal membranes, Phys. Rev. B **91**, 075414 (2015).
[38] Tuomas A. Puurtinen and Ilari J. Maasilta, Low-temperature coherent thermal conduction in thin phononic crystal membranes, Crystals **6**, 72 (2016).
[39] Roman Anufriev and Masahiro Nomura, Reduction of thermal conductance by coherent phonon scattering in two-dimensional phononic crystals of different lattice types, Phys. Rev. B **93**, 045410 (2016).
[40] Jongwoo Lim, Hung-Ta Wang, Jinyao Tang, Sean C. Andrews, Hongyun So, Jaeho Lee, Dong Hyun Lee, Thomas P. Russell, and Peidong Yang, Simultaneous thermoelectric property measurement and incoherent phonon transport in holey silicon, ACS Nano **10**, 124 (2016).
[41] Maxime Verdier, Roman Anufriev, Aymeric Ramiere, Konstantinos Termentzidis, and David Lacroix, Thermal conductivity of phononic membranes with aligned and staggered lattices of holes at room and low temperatures, Phys. Rev. B **95**, 205438 (2017).
[42] K. F. Graff, *Wave Motion in Elastic Solids* (Oxford University Press, London, 1975).
[43] T. Kühn, D. V. Anghel, J. P. Pekola, M. Manninen, and Y. M. Galperin, Heat transport in ultrathin dielectric membranes and bridges, Phys. Rev. B **70**, 125425 (2004).
[44] F. Giazotto, T. T. Heikkilä, A. Luukanen, A. M. Savin, and J. P. Pekola, Opportunities for mesoscopics in thermometry and refrigeration: Physics and applications, Rev. Mod. Phys. **78**, 217 (2006).
[45] P. J. Koppinen and I. J. Maasilta, Phonon Cooling of Nanomechanical Beams with Tunnel Junctions, Phys. Rev. Lett. **102**, 165502 (2009).
[46] M. M. Leivo and J. P. Pekola, Thermal characteristics of silicon nitride membranes at sub-kelvin temperatures, Appl. Phys. Lett. **72**, 1305 (1998).
[47] M. Meschke, W. Guichard, and J. P. Pekola, Single-mode heat conduction by photons, Nature (London) **444**, 187 (2006).
[48] Lord Rayleigh, On the influence of obstacles arranged in rectangular order upon the properties of a medium, Phil. Mag. **34**, 481 (1892).
[49] Luis G. C. Rego and George Kirczenow, Quantized Thermal Conductance of Dielectric Quantum Wires, Phys. Rev. Lett. **81**, 232 (1998).
[50] T. Kühn and I. J. Maasilta, Maximizing phonon thermal conductance for ballistic membranes, J. Phys.: Conf. Ser. **92**, 012082 (2007).
[51] See the Supplemental Material at http://link.aps.org/supplemental/10.1103/PhysRevApplied.12.014008 for the modeling of the effect of the heater and thermometer geometry, the modeling of the heat flow as a set of ballistic beams, and estimation of the effect of boundary roughness.
[52] Takuma Hori, Junichiro Shiomi, and Chris Dames, Effective phonon mean free path in polycrystalline nanostructures, Appl. Phys. Lett. **106**, 171901 (2015).
[53] Changwook Jeong, Supriyo Datta, and Mark Lundstrom, Full dispersion versus Debye model evaluation of lattice thermal conductivity with a Landauer approach, J. Appl. Phys. **109**, 073718 (2011).
[54] J. M. Ziman, *Electrons and Phonons* (Oxford University Press, Oxford, 1960).
[55] A. A. Maznev, Boundary scattering of phonons: Specularity of a randomly rough surface in the small-perturbation limit, Phys. Rev. B **91**, 134306 (2015).
[56] Dhruv Gelda, Marc G. Ghossoub, Krishna Valavala, Jun Ma, Manjunath C. Rajagopal, and Sanjiv Sinha, Specularity of longitudinal acoustic phonons at rough surfaces, Phys. Rev. B **97**, 045429 (2018).
[57] John R. Howell, Robert Siegel, and M. Pinar Menguc, *Thermal Radiation Transfer*, 5th ed. (CRC Press, Boca Raton, 2011).
[58] Ed. Ch. Enss, *Cryogenic Particle Detection* (Springer, Berlin, 2005).
[59] I. M. W. Räisänen, Z. Geng, K. M. Kinnunen, and I. J. Maasilta, Normal metal - insulator - superconductor thermometers and coolers with titanium-gold bilayer as the normal metal, J. Phys.: Conf. Ser. **969**, 012090 (2018).